DOI:
10.1016/j.jid.2019.01.037

Document Version
Peer reviewed version

DISRUPTION OF THE SENSORY SYSTEM AFFECTS STERILE CUTANEOUS INFLAMMATION *IN VIVO*

La Russa Federica[1*], Lopes Douglas M.[1], Hobbs Carl[1], Argunhan Fulye[2], Brain Susan[2], Bevan Stuart[1], Bennett David L.H.[3], McMahon Stephen B.[1]

[1] King's College London, Wolfson Centre for Age Related Diseases; [2] King's College London, School of Cardiovascular Medicine and Sciences; [3]Nuffield Department of Clinical Neurosciences, University of Oxford.

**Corresponding authors:* orcid.org/0000-0002-1885-6566; federica.la_russa@kcl.ac.uk; Dr Federica La Russa, Neurorestoration group, Wolfson Wing, Hodgkin Building, King's College London, Guy's Campus, London Bridge. London, SE1 1UL.

Abbreviations: CGRP: Calcitonin Gene-Related Peptide; DC: Dendritic Cell; dDC: dermal Dendritic Cell; LC: Langerhans Cell; mDC: monocyte-derived Dendritic Cell; mMΦ: monocyte-derived Macrophage; rMΦ: resident Macrophage; RTX: Resiniferatoxin; TRP: Transient Receptor Potential; KO: knock out

ABSTRACT

Increasing evidence suggests that nerve fibers responding to noxious stimuli (nociceptors) modulate immunity in a variety of tissues including the skin. Yet, a role for nociceptors in regulating sterile cutaneous inflammation remains unexplored. To tackle this question, we have developed a detailed description of the sterile inflammation caused by overexposure to UVB irradiation (*i.e.* sunburn) in the mouse plantar skin. Using this model, we observed that chemical depletion of nociceptor terminals did not alter the early phase of the inflammatory response to UVB, but it caused a significant increase in the number of dendritic cells and $\alpha\beta^+$ T cells as well as enhanced extravasation during the later stages of inflammation. Finally, we showed that such regulation was driven by the nociceptive neuropeptide Calcitonin Gene Related Peptide. In conclusion, we propose that nociceptors do not only play a crucial role in inflammation through avoidance reflexes and behaviors but can also regulate sterile cutaneous immunity *in vivo*.

INTRODUCTION

Nociceptors are multimodal sensory neurons, which detect and transduce a wide range of noxious stimuli applied to peripheral tissues. They transmit this information to the central nervous system where withdrawal responses and pain perception arise (Dubin and Patapoutian, 2010). There are two major classes of nociceptors, namely Aδ and C-fibers (Meyer, 2008). C-fibers can be further classified into two main subpopulations: peptidergic neurons, which release neuropeptides such as Substance P (SP) and Calcitonin Gene-Related Peptide (CGRP), and non-peptidergic neurons (Basbaum et al., 2009). Subpopulations of nociceptors can be also identified by the type of stimuli they respond to, due to the discrete expression of a combination of receptors and ion channels

including, for instance, the transient receptor potential (TRP) vanilloid 1 (TRPV1) and ankyrin1 (TRPA1) responding to capsaicin (*i.e.* active ingredient of chili pepper) or environmental irritants and inflammatory molecules, respectively (Woolf and Ma, 2007).

The skin, a prototypical neuroimmune organ, is densely innervated by nociceptors and is also highly populated by immune cells. This begs the question to what extent these two components might influence each other. Compelling studies have shown that nociceptors can acquire immunomodulatory properties in cutaneous homeostasis as well as in settings of pathological inflammation such as psoriasis, allergic dermatitis and infections (Beresford et al., 2004, Chiu et al., 2013, Girolomoni and Tigelaar, 1990, Kashem et al., 2015, Ostrowski et al., 2011, Riol-Blanco et al., 2014). Yet, a role for nociceptors in acute sterile inflammation has never been investigated and represents the focus of this work.

Sterile inflammation can be triggered by a wide range of stimuli, including overexposure to UVB irradiation. UVB-mediated inflammation is thought to cause distinctive alterations of both neuronal and immune cutaneous compartments, thus making this model ideal to investigate the interaction between neurons and immunity *in vivo*. UVB irradiation causes hyperactivation of nociceptors, which results in hyperalgesia (*i.e.* a condition where a painful stimulus is perceived as even more painful) in rodents and humans (Lopes and McMahon, 2016). UVB irradiation also triggers erythema and edema caused by a combination of neurogenic mechanisms along with a response to non-neuronal mediators such as reactive oxygen species (Clydesdale et al., 2001). Further, UVB light induces a dramatic alteration in skin composition and in epithelial and immune cell biology together with a profound change of the cutaneous *milieu* (Clydesdaleet al., 2001,

Dawes et al., 2014). Of note, changes in the immune compartment of the skin have been better described following repetitive exposure (either of the ear or the back skin) to low doses of UVB, which results in immunosuppression (Elmets et al., 2014). By contrast, immune alterations induced by a single exposure to high dose UVB light (as in sunburn) have never been characterized in-depth. Acute inflammation caused by UVB overexposure is thought to resolve three to four days after initiation, although the properties of such a resolution are still poorly investigated.

Here, we describe a setting of UVB-induced inflammation where, in contrast to earlier studies, both sensory and immunological cutaneous changes were simultaneously analyzed in the murine plantar skin. This system was employed to investigate the consequences of the disruption of the nociceptive signaling pathway during acute sterile cutaneous inflammation. Chemical denervation of the skin resulted in increased content of dendritic cells (DCs) as well as T cells following UVB irradiation and altered vascular integrity. Similarly, alterations in skin composition were observed following ablation of the nociceptive peptide CGRP in UVB inflammation. We therefore propose that nociceptors play a role in modulating immune responses in sterile cutaneous inflammation caused by UVB irradiation *in vivo*.

RESULTS

UVB irradiation causes neuronal and immune cell type-specific alterations *in vivo*

The aim of this study was to investigate how nociceptors may affect immune cells in cutaneous sterile inflammation. As a result, an in-depth characterization of the neuronal and immune alterations caused by acute exposure to high dose of UVB in the plantar skin was first performed (**Fig. 1; Fig. 2**).

We found a time-dependent and significant development of edema, which peaked at 48 hrs and had completely resolved by day 10 after UVB (**Fig. 1c**). At 48 hrs post exposure, erythema of the irradiated paw was also apparent (**Fig. 1b**). Furthermore, we observed a dramatic mechanical hyperalgesia mirroring widely accepted studies in humans and rats (Bishop et al., 2007, Saade et al., 2008). The mechanical hyperalgesia lasted up to 5d post UVB and had completely resolved by day 10 post exposure (**Fig. 1d**).

Composition of the murine plantar skin has been assessed by flow cytometry following automated dissociation. A specific gating strategy was adapted from Henri *et al.* to identify several subpopulations of immune cells, thus overcoming the limitations of previous histological studies, which looked only at a few immune cell types at the peak of inflammation (**Fig. 1S**) (Di Nuzzo et al., 1998, Henri et al., 2010, Kennedy Crispin et al., 2013, Meunier et al., 1995, Terui et al., 2001). Flow cytometry showed a time-dependent and significant increase of $CD45^+$ cells in the irradiated paw as compared to the non-irradiated skin (**Fig. 2a-b**). Infiltration of monocytes as well as neutrophils peaked between 48 and 72 hrs confirming earlier studies in both rodents and humans (Cooper et al., 1993, Teruiet al., 2001, Teunissen et al., 2002). Notably, we discriminated between monocyte-derived DCs and macrophages (mDCs and mMΦs respectively), not previously done in this model (**Fig. 2j, e, h**). At later time points, a significant increase of $\alpha\beta^+$ T cells was observed, supporting the idea of UVB causing infiltration and/or proliferation of these cells *in vivo* (Di Nuzzoet al., 1998, Teruiet al., 2001) (**Fig. 2c**). Interestingly, an increase of inflammatory DCs (herein mDCs) has been suggested to enhance T cell proliferation *in vivo* post UVB, and the kinetics of our data supports this possibility (Cooperet al., 1993) (**Fig. 2e, c**). Monocyte infiltration could also explain the observed increase of dermal DCs (dDCs) at later stages of inflammation, in agreement with studies proposing that recruited monocytes may mature into DCs within the skin

upon UVB (**Fig. 2f**) (Cooperet al., 1993). In contrast with previous reports proposing that Langerhans cells (LCs) undergo apoptosis or migration to the lymph nodes following irradiation, we saw a time-dependent increase in LCs (**Fig. 2g**) (Aberer et al., 1981, Zelickson and Mottaz, 1970). To our knowledge previously unreported, we looked at the effect of UVB on LCs in acute instead of tolerogenic responses, and this provides a likely explanation for such difference. Finally, the numbers of resident MΦs (rMΦs) as well as $\gamma\delta^+$ T cell did not significantly change over time (**Fig. 2i, d**). Yet, this observation does not exclude the possibility of alterations in the biology of these cells and would require further investigation.

Collectively, these data not only confirm the mechanical pain related hypersensitivity described in the previous literature, but also provide previously unreported insights on cell type-specific modification of cutaneous composition over time following acute exposure to UVB *in vivo*. This model was therefore considered suitable for testing the role of nociceptors in modulating immunity in sterile cutaneous inflammation.

Chemical denervation affects UVB-inflammation

We next asked whether cutaneous denervation might affect UVB-induced inflammation. Successful achievement of denervation of the plantar skin was confirmed behaviorally and histologically following administration of Resiniferatoxin (RTX) (**Fig. 2S a-c.**). High dose of RTX is indeed known to cause retraction of $TRPV1^+$ peptidergic fibres from the skin resulting in hyposensitivity to noxious stimuli (O'Neill et al., 2012). Publicly available datasets show that immune cells do not express *Trpv1*, suggesting that RTX only targets sensory neurons (Heng et al., 2008, Su et al., 2004). Similarly, we observed no expression of *Trpv1* in sorted cutaneous cell subpopulations in contrast to sensory neurons (**Fig. 2S d; Fig. 3f**).

Nociceptive hypersensitivity due to UVB irradiation developed as early as 24 hrs (data not shown), whereas immune changes in skin composition were not apparent prior to 48 hrs. In light of this, we hypothesized that nociceptors might modulate the initiation of the UVB-inflammation. To our surprise, this was not the case. RTX treated mice developed the same changes in immune cell composition of the skin as controls, suggesting that, in this type of inflammation, sensory innervation provides an acute defense mechanism which is purely behavioral in nature (**Fig. 3S a-c**). In contrast, when skin composition was evaluated at 5d post UVB irradiation, a significant increase in $CD45^+$ cells was observed in denervated skin compared to controls with a higher content of mDCs, rDCs and $\alpha\beta^+$ $CD4^+$ T cells (**Fig. 3a-c**). No difference was observed in edema at any time point tested (**Fig. 4S a**). The cellular alterations normalized by day 10 post exposure, suggesting a transitory nature of the observed phenotype (**Fig. 3S d-f**). RTX administration caused an unforeseen high mortality rate in male mice. The cause of such effect is unknown, and given the narrow therapeutic index in males, these experiments were only performed in female mice. Therefore, further studies are necessary to confirm if the phenotype observed in UVB inflammation is true for both genders.

Changes in the footpad were also assessed by qualitative histological analysis. At day 5 post UVB, both denervated and control skin showed focal areas of disruption of the epidermal-to-dermal interface with presence of hypertrophic and pyknotic cells. A milder grade of disruption was consistently noticeable in denervated skin, suggestive of a faster recovery from the cutaneous pathology caused by UVB (**Fig. 3d**). However, such difference could not be statistically evaluated and would require further analysis to be confirmed.

It has long been known that sensory innervation and nociceptive neuropeptides modulate vascular responses during neurogenic inflammation (Brain and Williams, 1989, Edvinsson et al., 1987). We

therefore asked whether alteration of vascular permeability may in part account for the phenotype observed in RTX treated mice. Data collected support this hypothesis showing that, at 5d post exposure to UVB, a significant extravasation was still ongoing in denervated skin when compared to controls (**Fig. 3e**). Our observation may appear hard to reconcile with the known ability of sensory innervation to induce vasodilation and vascular permeability, but several points need considering. Nociceptors are known to trigger neurogenic vascular responses acutely upon injury, but we observed our differences at a much later time point. Moreover, it has been shown that nociceptive neuropeptides may also suppress leakage and swelling in both rodents and humans (Clementi et al., 1995, Raud et al., 1991). It has also been proposed that edema upon UVB irradiation may result from a combination of neurogenic and non-neurogenic mechanisms, including a shift in the balance between pro and anti-angiogenic factors (Yano et al., 2004). Therefore, it may be possible that denervation might impact on such processes rather than directly on the vasculature permeability. Finally, our data may also reflect impaired drainage of the tissue, but, at this stage, no conclusion can be drawn.

Given the increase in the number of immune cells in the plantar skin, we also tested whether enhanced proliferation of immune cells might be a mechanism involved, but we did not see a difference in the frequencies of cells intercalating EdU between groups (**Fig. 2S e**).

Finally, in the attempt to pinpoint potential mediators involved in the phenotype observed, we evaluated the kinetics of transcriptional changes of chemokines in the plantar skin following UVB. Among the genes tested, the chemokines *Cxcl1* and *Cxcl3* showed a trend towards upregulation in RTX group compared to controls, supporting the possibility of increased chemoattraction in absence of sensory neurons (**Fig. 3g**).

To date, nociceptors have been shown to modulate cutaneous inflammation in pathological inflammatory conditions such as psoriasis, allergic contact dermatitis and upon infection (Beresfordet al., 2004, Chiuet al., 2013, Girolomoni and Tigelaar, 1990, Kashemet al., 2015, McMahon et al., 2015, Ostrowskiet al., 2011, Riol-Blancoet al., 2014). Collectively, our data suggest that nociceptors also affect UVB-mediated changes in terms of immune cell composition and tissue integrity following irradiation *in vivo*.

TRPA1 or TRPV1 are not sufficient to mediate UVB-changes

The ways by which UVB irradiation causes hyperactivation of sensory innervation are not well defined. It has however been shown that UVB causes upregulation of TRPV1, and that TRPV1 is crucial for the hyperalgesia following UVB irradiation (Chizh et al., 2007, Sisignano et al., 2013). Furthermore, TRPV1 as well as TRPA1 are known to detect inflammatory mediators, which are abundantly expressed following UVB irradiation *in vivo* (Andersson et al., 2008, Sisignanoet al., 2013, Trevisani et al., 2007). We therefore asked whether TRP channels expressed by nociceptors might contribute to the modulation of the UVB-inflammation. Ablation of *Trpv1* did not affect UVB-mediated changes in cutaneous composition at day 5 post irradiation (**Fig. 4a-c**). Instead, it appears that loss of function or pharmacological blockade of TRPA1 caused small, but not significant, alterations similar to those induced by chemical denervation (**Figure 4d-i**).

These observations suggest that, while TRPA1 could play a minor role, ultimately both TRPV1 and TRPA1 are dispensable for nociceptor-mediated modulation of UVB-inflammation. Upon UVB irradiation a plethora of inflammatory mediators are released in the skin and these can signal through a great variety of receptors expressed by sensory innervation. It is therefore possible that

neurons lacking *Trpv1* or *Trpa1* would maintain a sufficient degree of activities and compensate for the discrete ablation of these specific ion channels.

Ablation of CGRP affects UVB-inflammation

Upon activation, nociceptors release a variety of mediators including neuropeptides such as CGRP and SP, which have been shown to play a role in neuroimmune interactions in a variety of experimental settings (!!! INVALID CITATION !!! , McMahonet al., 2015). So far, CGRP has attracted most of the attention in the field of cutaneous neuroimmunology and, of relevance to this study, it is upregulated in the skin upon irradiation (Granstein et al., 2015, Scholzen et al., 1999). Therefore, we asked whether CGRP may play a role in modulating UVB-inflammation. Analysis of skin composition in *Cgrp-α* knock out (KO) mice revealed a comparable pattern of changes to those observed in denervated mice. We saw a significant increase in $CD45^+$ cells due to a higher number of DCs and $\alpha\beta^+$ T cells in KO mice compared to controls (**Fig. 5a-c**). In line with the phenotype observed, analysis of publicly available datasets showed that murine DCs and T cell as well as human DCs express the receptor for CGRP (*Ramp1/*RAMP1) to varying degrees while lacking the neuropeptide itself (**Fig. 5d-e**) (Henget al., 2008, Stunnenberg et al., 2016). Further, recent studies have shown that CGRP can indeed modulate the biology of cutaneous DCs *in vivo* (Kashemet al., 2015, Riol-Blancoet al., 2014). Similar to the data collected from RTX-treated mice and controls, we did not observe any difference edema at any time point tested (**Fig. 4S b**). Further, the observed immune-related phenotype did not impact the mechanical hyperalgesia in *Cgrp-α* KO compared to controls (**Fig. 4S c**).

The functional consequences of the neuronal mediated immunomodulation via CGRP have been shown to vary depending on the pathological setting taken into consideration. For instance, in

experimental models of pathological inflammation such as psoriasis and upon *Candida albicans* infection, CGRP has been shown to be functionally detrimental. By contrast, other studies support the hypothesis of CGRP being immunosuppressive in allergic inflammatory reactions (Gomes et al., 2005, Gransteinet al., 2015, Hosoi et al., 1993, Levite and Chowers, 2001, Mikami et al., 2011, Torii et al., 1997). In light of this, further investigation will be essential to understand whether the increase in the content of immune cells upon neuronal or CGRP disruption is functionally detrimental or protective for the sterile inflammation caused by UVB, with our histological observation suggesting the first might be the case.

To conclude, we have shown that not only do nociceptors provide a means to limit skin injury and promote repair through mediating behavioral responses, but also play a role in modulating cutaneous biology in sterile inflammation through the neuropeptide CGRP.

MATERIALS AND METHODS

Mice

C57BL/6J female mice were provided by Envigo, *Trpa1, Trpv1* KO and *Cgrp-α* KO female mice were kindly provided by Stuart Bevan and Susan Brain, respectively (Kwan et al., 2006, Smillie et al., 2014). All control mice for knock out experiments were wild type animals. To limit variability between the cohorts, mice have been co-housed in the same facility either from birth (in case of the *Cgrp-α* KO mice) or at least for two weeks before performing further experiments. Mice were used at 8-10 week of age or at 4-week when dosed with RTX. All experiments were performed in agreement with the United Kingdom Home Office legislation (Scientific Procedures Act 1986). Food and water were available *ad libitum*, and animals were housed under standard conditions with a 12-hour light/dark cycle.

UVB irradiation of plantar skin

Mice were fully anaesthetized (0.25 mg/kg Dormitor (Orion Pharma), and 60 mg/kg Ketamin (Zoetis) delivered intraperitoneally) and completely covered except for the plantar side of one hind paw. Animals were then transferred into a chamber equipped with TL01 fluorescent bulbs (maximum wavelength 311nm), and the plantar skin exposed to 3000 mJ/cm^2 of UVB light. Before each irradiation, UVB light intensity (UI) was measured with a photometer placed at the same distance of the exposed skin. This reading was used to calculate the time required to deliver the desired intensity with the following formula: time (min) = 3000 mJ/ UI mW / 60. After the procedure, animals were recovered by subcutaneous injection of atipamezole hydrochloride (1 mg/kg, Orion Pharma) followed by saline (1 ml/mouse).

Von Frey testing

Von Frey test assesses sensitivity to mechanical stimulation. Mice were singly housed into chambers placed on a mesh platform and left to acclimatize until exploratory and grooming activity ceased. Paw withdrawal was assessed using the up-down paradigm to determine at what pressure the mice respond 50% of the stimulation (Chaplan et al., 1994). Briefly, each animal was stimulated with the 0.6 g first. In the absence of a response, a stronger stimulus was applied, whereas in presence of paw withdrawal the consecutive weaker hair was presented. The resulting pattern of positive and negative responses was tabulated using the following convention, X = withdrawal; O = no withdrawal. The 50% response threshold was interpolated using the following formula: 50% g threshold = $(10^{[Xf+k\delta]})/10.000$, where X_f = value of the final von Frey hair used

(log units); k = tabular value for the pattern of positive/negative responses (list not provided here); and δ = mean difference between stimuli (here, 0.224).

Paw thickness assessment

Paw thickness at the mid-plantar surface was measured with a digital thickness gauge [range 0-25.4 mm] upon restraining of awake mice.

Processing and flow cytometry of plantar skin

Mice were sacrificed by overdose of anesthetic and transcardially perfused with 10-20 ml of phosphate buffer saline (PBS). Plantar skin was collected, minced and incubated into a digestion cocktail [400 μg/ml Liberase TL grade (Roche, #05401020001), 30 μg/ml DNase (Roche, #11284932001) in DMEM Glutamax (Gibco, 10566-016)] for 2.5 hrs at 37 °C in agitation. Samples were then mechanically dissociated in gentle MACS C-tubes (Miltenyi Biotech, #130-093-237) after adding an equal volume of DMEM supplemented with 10% foetal bovine serum (FBS) (Gibco, #10082147). Following dissociation, the obtained suspension was passed through a 70 μm cell strainer, cells centrifuged (10 min, 1800 rpm, RT), resuspended in 200 μl of FACS buffer [HBSS (Gibco, #14025092) supplemented with 5% bovine serum albumin (BSA) (Sigma, #A2058), 10 mM Hepes (Gibco, #15630080) and 2 mM EDTA (Gibco, #15575020)] and transferred into a 96 multi-well V bottom plate for staining. Samples were then incubated with a viability dye (Life Technologies, #L34963/L34967) for 30 min, washed and re-suspended in a cocktail of several antibodies prepared in FACS buffer supplemented with a 1:20 diluted FcR blocking solution (Biolegend, #101301). Following a 30 min incubation, samples were washed with FACS buffer, fixed in 4% PFA (Sigma, #F8775) for 3 min, washed, resuspended and left in

FACS buffer until acquisition. Unstained cells, cells stained only with viability dye and single staining controls as beads (BD Biosciences, #552845) were used to ensure optimal compensation. Anti-mouse antibodies (all Biolegend) used were the following: αβ TCR (PE, PE-Cy7-conjugated, clone H57-597); γδ TCR (APC-conjugated, clone GL3); CD11b (Pacific Blue, PerCP-Cy5.5, APC-Cy7-conjugated, clone M1/70); CD24 (PE-conjugated, clone 30-F1), CD4 (APC-Cy7-conjugated, clone GK1.5), CD45 (FITC-conjugated, clone 30-F11), CD8 (PE-Cy7-conjugated, clone 53-6.7), Ly6C (BV711-conjugated, clone HK1.4), Ly6G (Pacific Blue-conjugated, clone 1A8), MHCII (PE-Cy7, PerCP-Cy5.5-conjugated, clone M5/114.15.2). Discrimination of immune cell subpopulations in plantar skin preparation was achieved as shown in **Fig.1S,** where a myeloid or lymphoid-specific panel was used to stain half of each sample. Flow cytometry was performed on a BD FACS Fortessa (BD Pharmingen) and data analyzed using Flowjo software (Treestar).

Sort of plantar skin cell subpopulations

Plantar skin of naïve mice was collected, processed, stained as described above except for PFA incubation. Discrimination of cutaneous cell subpopulations was achieved following the gating strategy shown in **Fig 2S d**. Cell sorts were performed on a BD FACS Aria II (BD Pharmingen).

Chemical denervation

4-week-old female C57BL/6J mice were administered increasing subcutaneous doses (10>30>60 μg/kg) of RTX (Sigma, #57444-62-9) or vehicle (EtOH 100%, Sigma, # 459836) over three consecutive days. Animals were recovered for three to four weeks before performing any further procedure.

Hot plate

Hot plate test assesses sensitivity to noxious thermal stimulation. Mice were placed on a hot plate at 52 °C and the latency of withdrawal responses measured with a cut-off time of 40 sec.

Nerve density quantification and histopathology of the skin

Plantar skin was collected as described above and post-fixed in 4% PFA overnight at 4 °C. Following 48 hrs cryoprotection in 20% sucrose, biopsies were embedded in OCT. 10 μm cryostat cut sections were then thaw-mounted onto glass gelatine pre-coated slides. For nerve density quantification, skin sections were incubated overnight with the primary antibody rabbit anti-PGP9.5 (1:2000, Ultraclone, #RA95101), followed by a 3 hr incubation with a secondary antibody anti-rabbit IgG Cy3-conjugated (1:500, Stratech, #43R-IM001C3-FIT). Intraepidermal fibers were visualized and manually counted following previously published guidelines and the intraepidermal nerve fiber density quantified as *ratio* between average of number of fibers counted and average length of analysed sections (three/biopsy) (Lauria et al., 2005). For histopathology, sections were incubated with haematoxylin (Millipore #1.05175.0500) following a re-hydration step. Upon wash in acid alcohol and water, the slides were exposed to eosin (Millipore #1.15935.0025). Finally, samples were dehydrated through exposure to graded alcohols (80-90-95-100%) and cleared in Xylene (Sigma #1330-20-7). Scoring of the sections was performed blinded to the treatment groups looking at presence of epithelial layer disruption as well as hypertrophic and pyknotic cells.

Administration of the TRPA1 antagonist Chembridge-5861528

Mice were administered 40 mg/kg of Chembridge-5861528 or 0.5% Methyl cellulose by oral gavage twice daily from the day of irradiation until sacrifice.

RNA extraction and RT-q PCR of skin and cutaneous sorted cells

Plantar skin was collected as described above, snap frozen and stored at -80° C until RNA extraction when each biopsy was homogenized in 500 µl of Trizol (Ambion, #15596026). Suspensions were then mixed with 100 µl of chloroform (Sigma, #C2432) and transferred to a phase gel lock column (Qiagen, #2900309). Upon centrifugation (15 min, 12000 rpm, 4 °C), the aqueous phase was transferred into a fresh tube and extraction performed using the RNAeasy Plus Mini kit (Qiagen, #74134) following manufacturer instruction. Sorted cells were pelleted, resuspended in RLT buffer (Qiagen, #79216) and stored at -80° C until extraction with the RNAeasy Plus Mini kit. cDNA synthesis for RNA extracted from plantar skin was performed using Superscript III First-Strand Synthesis SuperMix kit (Invitrogen, #18080400) and random primers (Promega, #C1181). cDNA synthesis and amplification for RNA extracted from sorted cells was instead performed using the WTA repli-g (Qiagen, #150065). Finally, RT-qPCR reactions were run in 384-well plates on a LightCycler 480 (Roche) and cDNA amplified 40 times.

Evans blue assay

Mice were intravenously injected with 1% Evans blue. After 30 min, animals were sacrificed with an overdose of anesthesia and plantar skin collected as previously described. Skin biopsies were weighed, transferred into 500 µl of formamide (Sigma, #F7508) and incubated overnight at 65 °C. Evans blue concentration was obtained by measuring absorbance of supernatant at 650 nm, and content of Evans blue calculated as total amount of dye/mg of tissue collected.

Statistical analysis

Data are plotted as Mean ± Standard Error of the Mean (SEM) and were tested for normality distribution with the Shapiro-Wilk test. If data failed the normality test, non-parametric statistical tests were applied. All statistical analyses were performed using GraphPad.

DATA AVAILABILITY

Raw data that underlie the results reported in the main figures of this paper are made available to anyone who wishes to access them for any type of follow-up analysis. Data are indefinitely available after publication at the following link:

https://data.mendeley.com/datasets/2ptsj44wx5/draft?a=eec21a07-cd07-4fcf-94f2-80749e9dd081

CONFLICT OF INTEREST

The authors declare no competing financial interest.

ACKNOWLEDGEMENTS

This research for this project was financially supported by the Wellcome Trust, grant #083259/B/07/C and #097903/z/11/z. F.A. is an MRC-DTP Ph.D. student. The authors would like to thank the flow cytometry core facility at the Biomedical Research Centre, Guy's and St Thomas' NHS foundation trust, at King's College London. The authors would also like to thank Dr Matteo Villa (Max Plank Institute, Freiburg) for providing invaluable technical and conceptual advice and Dr Franziska Denk (King's College London) for her insights, which greatly assisted the research and the writing of the manuscript.

REFERENCES

Aberer W, Schuler G, Stingl G, Honigsmann H, Wolff K. Ultraviolet light depletes surface markers of Langerhans cells. J Invest Dermatol 1981;76(3):202-10.

Andersson DA, Gentry C, Moss S, Bevan S. Transient receptor potential A1 is a sensory receptor for multiple products of oxidative stress. J Neurosci 2008;28(10):2485-94.

Basbaum AI, Bautista DM, Scherrer G, Julius D. Cellular and molecular mechanisms of pain. Cell 2009;139(2):267-84.

Beresford L, Orange O, Bell EB, Miyan JA. Nerve fibres are required to evoke a contact sensitivity response in mice. Immunology 2004;111(1):118-25.

Bishop T, Hewson DW, Yip PK, Fahey MS, Dawbarn D, Young AR, et al. Characterisation of ultraviolet-B-induced inflammation as a model of hyperalgesia in the rat. Pain 2007;131(1-2):70-82.

Brain SD, Williams TJ. Interactions between the tachykinins and calcitonin gene-related peptide lead to the modulation of oedema formation and blood flow in rat skin. Br J Pharmacol 1989;97(1):77-82.

Chaplan SR, Bach FW, Pogrel JW, Chung JM, Yaksh TL. Quantitative assessment of tactile allodynia in the rat paw. J Neurosci Methods 1994;53(1):55-63.

Chiu IM, Heesters BA, Ghasemlou N, Von Hehn CA, Zhao F, Tran J, et al. Bacteria activate sensory neurons that modulate pain and inflammation. Nature 2013;501(7465):52-7.

Chizh BA, O'Donnell MB, Napolitano A, Wang J, Brooke AC, Aylott MC, et al. The effects of the TRPV1 antagonist SB-705498 on TRPV1 receptor-mediated activity and inflammatory hyperalgesia in humans. Pain 2007;132(1-2):132-41.

Clementi G, Caruso A, Cutuli VM, Prato A, de Bernardis E, Fiore CE, et al. Anti-inflammatory activity of amylin and CGRP in different experimental models of inflammation. Life Sci 1995;57(14):PL193-7.

Clydesdale GJ, Dandie GW, Muller HK. Ultraviolet light induced injury: immunological and inflammatory effects. Immunol Cell Biol 2001;79(6):547-68.

Cooper KD, Duraiswamy N, Hammerberg C, Allen E, Kimbrough-Green C, Dillon W, et al. Neutrophils, differentiated macrophages, and monocyte/macrophage antigen presenting cells infiltrate murine epidermis after UV injury. J Invest Dermatol 1993;101(2):155-63.

Dawes JM, Antunes-Martins A, Perkins JR, Paterson KJ, Sisignano M, Schmid R, et al. Genome-wide transcriptional profiling of skin and dorsal root ganglia after ultraviolet-B-induced inflammation. PLoS One 2014;9(4):e93338.

Di Nuzzo S, Sylva-Steenland RM, de Rie MA, Das PK, Bos JD, Teunissen MB. UVB radiation preferentially induces recruitment of memory CD4+ T cells in normal human skin: long-term effect after a single exposure. J Invest Dermatol 1998;110(6):978-81.

Dubin AE, Patapoutian A. Nociceptors: the sensors of the pain pathway. J Clin Invest 2010;120(11):3760-72.

Edvinsson L, Ekman R, Jansen I, McCulloch J, Uddman R. Calcitonin gene-related peptide and cerebral blood vessels: distribution and vasomotor effects. Journal of cerebral blood flow and metabolism : official journal of the International Society of Cerebral Blood Flow and Metabolism 1987;7(6):720-8.

Elmets CA, Cala CM, Xu H. Photoimmunology. Dermatol Clin 2014;32(3):277-90, vii.

Girolomoni G, Tigelaar RE. Capsaicin-sensitive primary sensory neurons are potent modulators of murine delayed-type hypersensitivity reactions. J Immunol 1990;145(4):1105-12.

Gomes RN, Castro-Faria-Neto HC, Bozza PT, Soares MB, Shoemaker CB, David JR, et al. Calcitonin gene-related peptide inhibits local acute inflammation and protects mice against lethal endotoxemia. Shock 2005;24(6):590-4.

Granstein RD, Wagner JA, Stohl LL, Ding W. Calcitonin gene-related peptide: key regulator of cutaneous immunity. Acta Physiol (Oxf) 2015;213(3):586-94.

Heng TS, Painter MW, Immunological Genome Project C. The Immunological Genome Project: networks of gene expression in immune cells. Nat Immunol 2008;9(10):1091-4.

Henri S, Poulin LF, Tamoutounour S, Ardouin L, Guilliams M, de Bovis B, et al. CD207+ CD103+ dermal dendritic cells cross-present keratinocyte-derived antigens irrespective of the presence of Langerhans cells. J Exp Med 2010;207(1):189-206.

Hosoi J, Murphy GF, Egan CL, Lerner EA, Grabbe S, Asahina A, et al. Regulation of Langerhans cell function by nerves containing calcitonin gene-related peptide. Nature 1993;363(6425):159-63.

Kashem SW, Riedl MS, Yao C, Honda CN, Vulchanova L, Kaplan DH. Nociceptive Sensory Fibers Drive Interleukin-23 Production from CD301b+ Dermal Dendritic Cells and Drive Protective Cutaneous Immunity. Immunity 2015;43(3):515-26.

Kennedy Crispin M, Fuentes-Duculan J, Gulati N, Johnson-Huang LM, Lentini T, Sullivan-Whalen M, et al. Gene profiling of narrowband UVB-induced skin injury defines cellular and molecular innate immune responses. J Invest Dermatol 2013;133(3):692-701.

Kwan KY, Allchorne AJ, Vollrath MA, Christensen AP, Zhang DS, Woolf CJ, et al. TRPA1 contributes to cold, mechanical, and chemical nociception but is not essential for hair-cell transduction. Neuron 2006;50(2):277-89.

Lauria G, Cornblath DR, Johansson O, McArthur JC, Mellgren SI, Nolano M, et al. EFNS guidelines on the use of skin biopsy in the diagnosis of peripheral neuropathy. Eur J Neurol 2005;12(10):747-58.

Levite M, Chowers Y. Nerve-driven immunity: neuropeptides regulate cytokine secretion of T cells and intestinal epithelial cells in a direct, powerful and contextual manner. Ann Oncol 2001;12 Suppl 2:S19-25.

Lopes DM, McMahon SB. Ultraviolet Radiation on the Skin: A Painful Experience? CNS Neurosci Ther 2016;22(2):118-26.

McMahon SB, La Russa F, Bennett DL. Crosstalk between the nociceptive and immune systems in host defence and disease. Nat Rev Neurosci 2015;16(7):389-402.

Meunier L, Bata-Csorgo Z, Cooper KD. In human dermis, ultraviolet radiation induces expansion of a CD36+ CD11b+ CD1- macrophage subset by infiltration and proliferation; CD1+ Langerhans-like dendritic antigen-presenting cells are concomitantly depleted. J Invest Dermatol 1995;105(6):782-8.

Meyer RA. Peripheral mechanisms of cutaneous nociception. . Wall and Melzack's Textbook of Pain, SB McMahon and M Koltzenburg, eds (Philadelphia:Elsevier) 2008:3-34.

Mikami N, Matsushita H, Kato T, Kawasaki R, Sawazaki T, Kishimoto T, et al. Calcitonin gene-related peptide is an important regulator of cutaneous immunity: effect on dendritic cell and T cell functions. J Immunol 2011;186(12):6886-93.

O'Neill J, Brock C, Olesen AE, Andresen T, Nilsson M, Dickenson AH. Unravelling the mystery of capsaicin: a tool to understand and treat pain. Pharmacol Rev 2012;64(4):939-71.

Ostrowski SM, Belkadi A, Loyd CM, Diaconu D, Ward NL. Cutaneous denervation of psoriasiform mouse skin improves acanthosis and inflammation in a sensory neuropeptide-dependent manner. J Invest Dermatol 2011;131(7):1530-8.

Raud J, Lundeberg T, Brodda-Jansen G, Theodorsson E, Hedqvist P. Potent anti-inflammatory action of calcitonin gene-related peptide. Biochem Biophys Res Commun 1991;180(3):1429-35.

Riol-Blanco L, Ordovas-Montanes J, Perro M, Naval E, Thiriot A, Alvarez D, et al. Nociceptive sensory neurons drive interleukin-23-mediated psoriasiform skin inflammation. Nature 2014;510(7503):157-61.

Saade NE, Farhat O, Rahal O, Safieh-Garabedian B, Le Bars D, Jabbur SJ. Ultra violet-induced localized inflammatory hyperalgesia in awake rats and the role of sensory and sympathetic innervation of the skin. Brain Behav Immun 2008;22(2):245-56.

Scholzen TE, Brzoska T, Kalden DH, O'Reilly F, Armstrong CA, Luger TA, et al. Effect of ultraviolet light on the release of neuropeptides and neuroendocrine hormones in the skin: mediators of photodermatitis and cutaneous inflammation. J Investig Dermatol Symp Proc 1999;4(1):55-60.

Sisignano M, Angioni C, Ferreiros N, Schuh CD, Suo J, Schreiber Y, et al. Synthesis of lipid mediators during UVB-induced inflammatory hyperalgesia in rats and mice. PLoS One 2013;8(12):e81228.

Smillie SJ, King R, Kodji X, Outzen E, Pozsgai G, Fernandes E, et al. An ongoing role of alpha-calcitonin gene-related peptide as part of a protective network against hypertension, vascular hypertrophy, and oxidative stress. Hypertension 2014;63(5):1056-62.

Stunnenberg HG, International Human Epigenome C, Hirst M. The International Human Epigenome Consortium: A Blueprint for Scientific Collaboration and Discovery. Cell 2016;167(7):1897.

Su AI, Wiltshire T, Batalov S, Lapp H, Ching KA, Block D, et al. A gene atlas of the mouse and human protein-encoding transcriptomes. Proc Natl Acad Sci U S A 2004;101(16):6062-7.

Terui T, Takahashi K, Funayama M, Terunuma A, Ozawa M, Sasai S, et al. Occurrence of neutrophils and activated Th1 cells in UVB-induced erythema. Acta Derm Venereol 2001;81(1):8-13.

Teunissen MB, Piskin G, di Nuzzo S, Sylva-Steenland RM, de Rie MA, Bos JD. Ultraviolet B radiation induces a transient appearance of IL-4+ neutrophils, which support the development of Th2 responses. J Immunol 2002;168(8):3732-9.

Torii H, Hosoi J, Beissert S, Xu S, Fox FE, Asahina A, et al. Regulation of cytokine expression in macrophages and the Langerhans cell-like line XS52 by calcitonin gene-related peptide. J Leukoc Biol 1997;61(2):216-23.

Trevisani M, Siemens J, Materazzi S, Bautista DM, Nassini R, Campi B, et al. 4-Hydroxynonenal, an endogenous aldehyde, causes pain and neurogenic inflammation through activation of the irritant receptor TRPA1. Proc Natl Acad Sci U S A 2007;104(33):13519-24.

Woolf CJ, Ma Q. Nociceptors--noxious stimulus detectors. Neuron 2007;55(3):353-64.

Yano K, Kajiya K, Ishiwata M, Hong YK, Miyakawa T, Detmar M. Ultraviolet B-induced skin angiogenesis is associated with a switch in the balance of vascular endothelial growth factor and thrombospondin-1 expression. J Invest Dermatol 2004;122(1):201-8.

Zelickson AS, Mottaz J. The effect of sunlight on human epidermis. A quantitative electron microscopic study of dendritic cells. Arch Dermatol 1970;101(3):312-5.

FIGURE

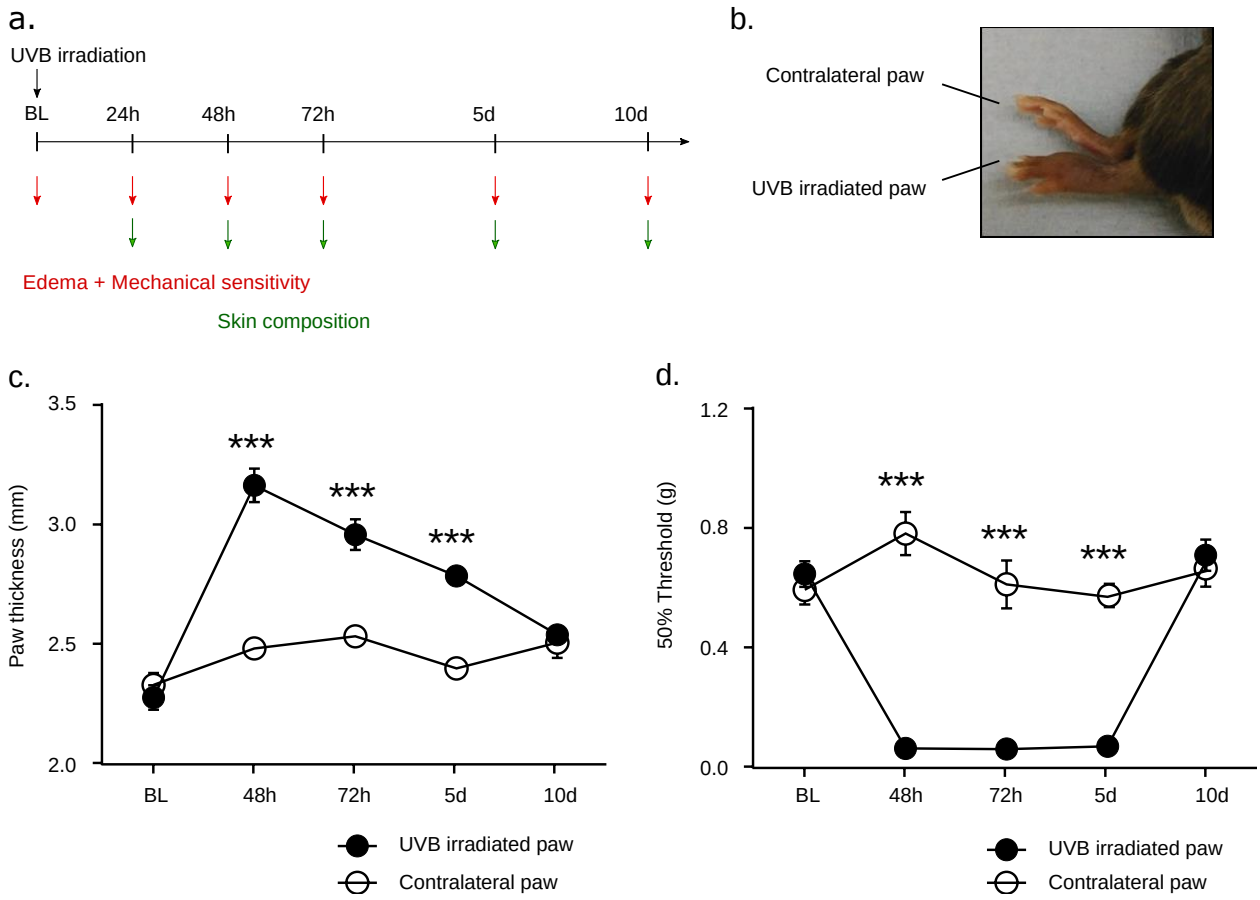

Figure 1. UVB irradiation causes time-dependent edema and mechanical hyperalgesia *in vivo*. **a.** Experimental timeline with edema, mechanical hyperalgesia and immune cutaneous composition tested at both acute (24-72 hrs) and later time points (5-10 d) following exposure. **b.** Representative image taken at 48 hrs post UVB exposure with irradiated paw showing edema and erythema. **c.** Time course of changes in edema measured as paw thickness. **d.** Time course of changes in sensitivity to mechanical stimulation measured as the amount of pressure required to induce withdrawal of the tested paw in 50% of the assessment. Data plotted as Mean ± SEM with n=8 mice/time point and representative of two independent experiments. Two-Way ANCOVA with repeated measures and baseline (BL) as co-variate followed by Bonferroni *post hoc* correction for multiple comparisons: ***: *p*-value < 0.0001.

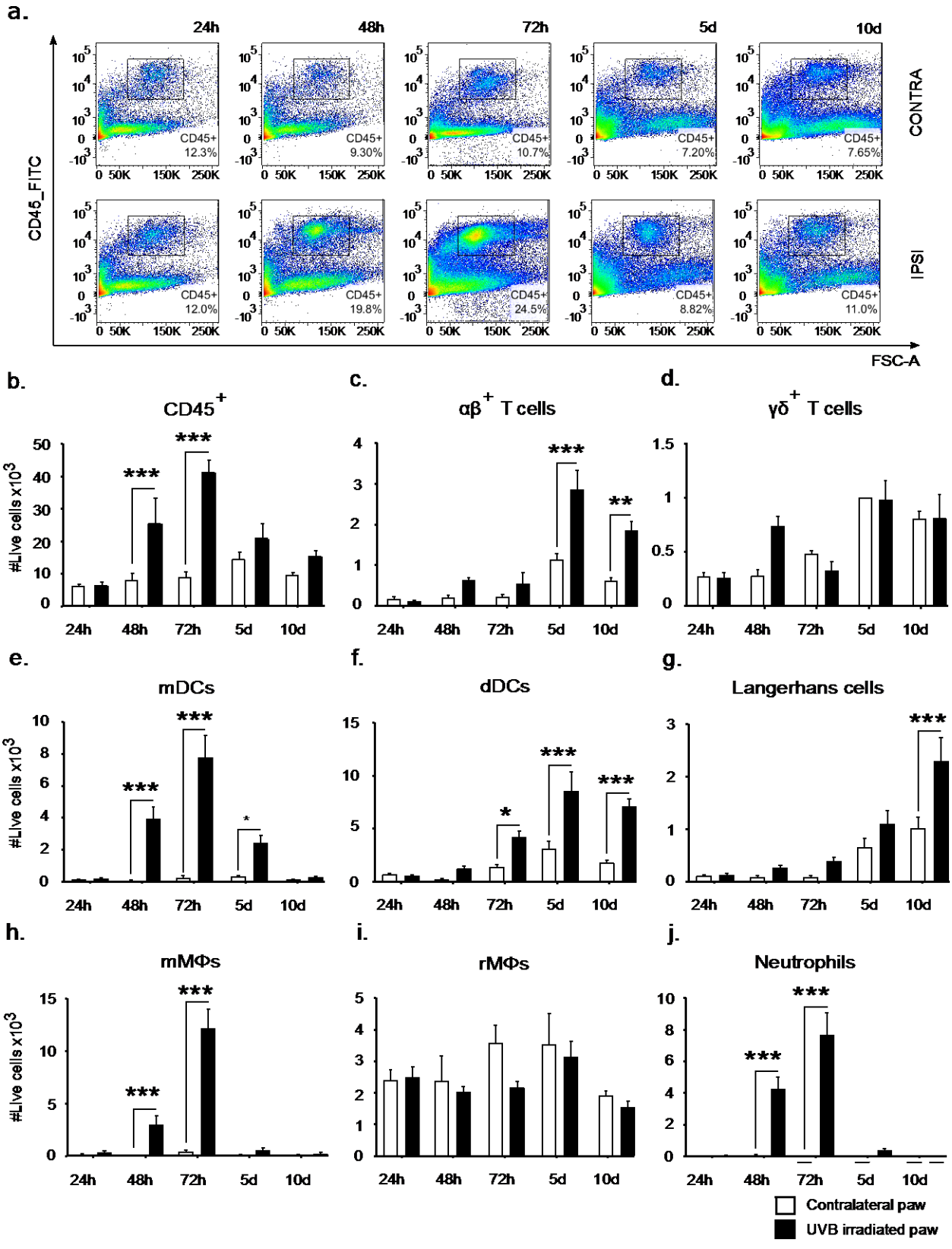
a.
24h
48h
72h
5d
10d
CONTRA
IPSI
CD45_FITC
FSC-A
CD45+ 12.3%
CD45+ 9.30%
CD45+ 10.7%
CD45+ 7.20%
CD45+ 7.65%
CD45+ 12.0%
CD45+ 19.8%
CD45+ 24.5%
CD45+ 8.82%
CD45+ 11.0%
b.
CD45+
c.
αβ+ T cells
d.
γδ+ T cells
e.
mDCs
f.
dDCs
g.
Langerhans cells
h.
mMΦs
i.
rMΦs
j.
Neutrophils
#Live cells x10^3
Contralateral paw
UVB irradiated paw

Figure 2. UVB irradiation causes time-dependent and cell-type specific alterations in the composition of the plantar skin *in vivo*. a. Representative flow cytometry dot plots showing the content of immune cells ($CD45^+$) in the irradiated (ipsi) and non-irradiated skin (contra). **b.** Flow cytometry quantification of the kinetics of changes of immune cell numbers following UVB compared to the non-irradiated side. **c-j.** Flow cytometry quantification of the kinetics of changes of specific immune cell subpopulations including lymphoid (c-d.) and myeloid (e-j.) cells in irradiated and contralateral skin. Gating strategy is provided in Fig. 1S. Data are plotted as Mean ± SEM with n=5 mice/time point and are representative of three independent experiments. Multiple unpaired t-test with Holm Sidak *post hoc* corrections for multiple comparisons: *: *p*-value < 0.05; *** *p*-value < 0.001. d: dermal; DCs: dendritic cells; m: monocyte-derived; MΦs: macrophages; r: resident.

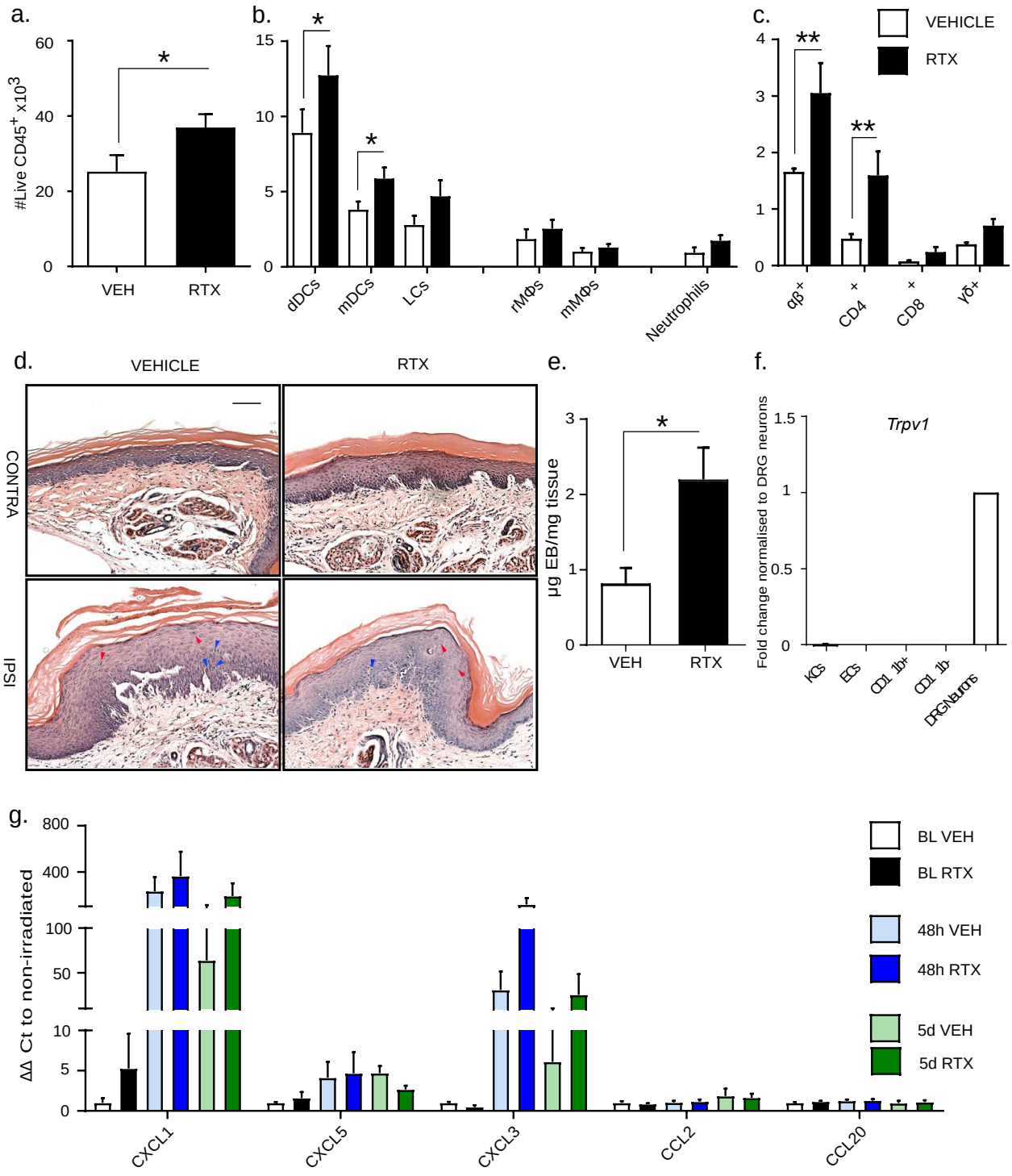

Figure 3. Chemical denervation affects changes in skin composition and extravasation caused by UVB irradiation *in vivo*. a-c. Flow cytometry analysis of cutaneous composition 5d post UVB in denervated and control mice. **d.** Representative pictures of hematoxylin-eosin

staining of footpad taken from RTX and vehicle-treated mice 5 days post UVB irradiation. Red arrow indicates hypertrophic cells whereas blue arrows point to pyknotic cells. Scale bar = 100μm. **e.** Assessment of extravasation by Evans blue assay in plantar skin performed at 5d post UVB. **f.** RT-qPCR quantification of *Trpv1* (RTX receptor) expression in different cutaneous subpopulations normalized to the expression in sensory neurons. **g.** RT-qPCR quantification of chemokines in whole plantar skin from denervated and control mice. Data plotted as Mean ± SEM with n=6 mice/group representative of three independent experiments (a-c.); n=4 mice/group (d.); n=8 mice/group pooled from two independent experiments (e.); n=4 mice (f.); and n=3 mice/group/time point (g.). Multiple unpaired t-test with Holm-Sidak *post hoc* correction for multiple comparisons: *: p-value<0.05; **: p-value<0.01. (b-c.). Unpaired t-test: *: p-value < 0.05 (a;e). d: dermal; DCs: dendritic cells; LC: Langerhans cells; m: monocyte-derived; MΦs: macrophages; r: resident.

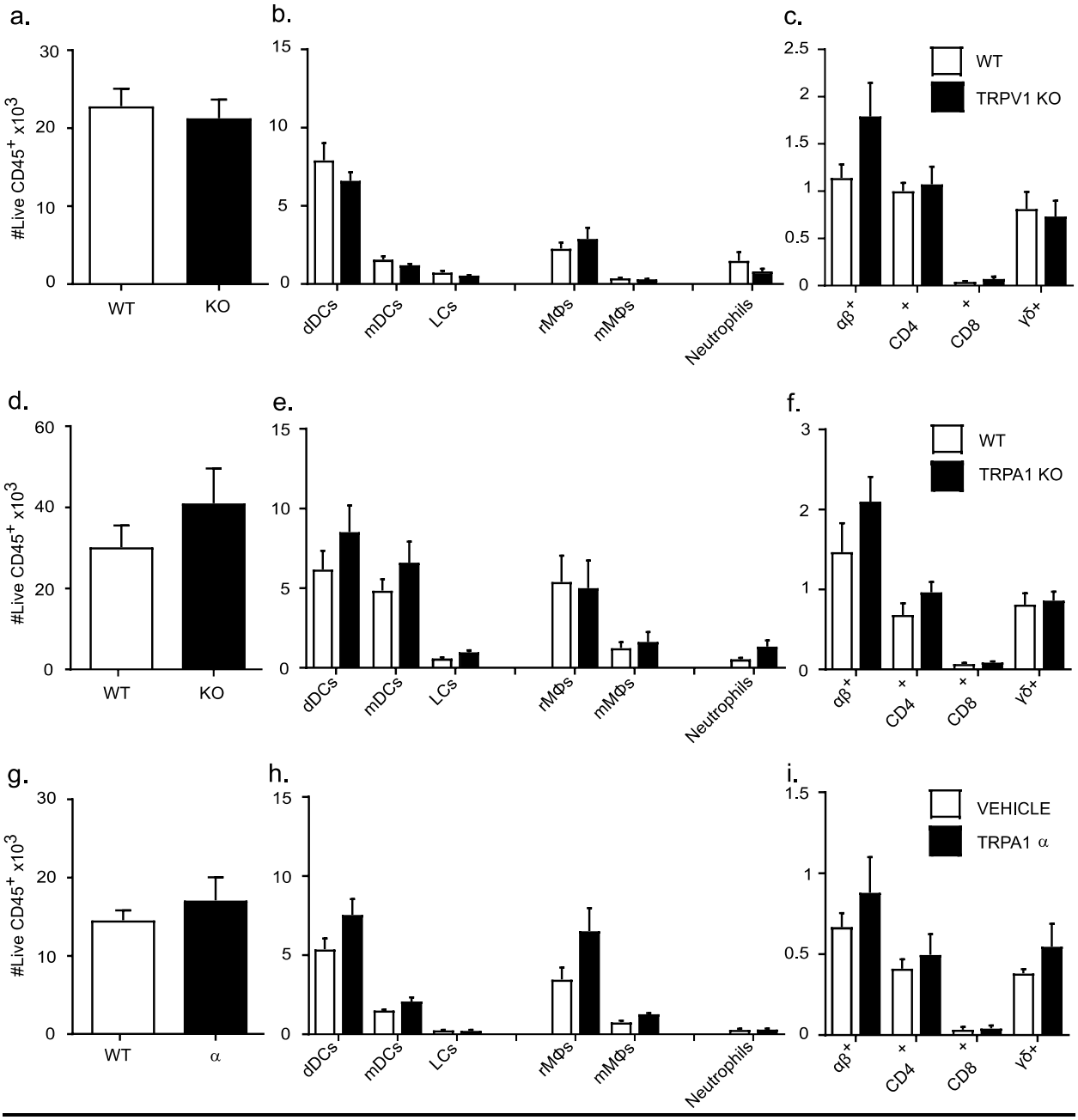

Figure 4. TRPV1 and TRPA1 do not play a role in modulating the alterations caused by UVB at day 5 post irradiation. **a-c.** Flow cytometry quantification of the content of immune cells and immune subpopulations in the plantar skin at day 5 post UVB exposure in TRPV1 KO and wild type mice. **d-f.** Flow cytometry quantification of the content of immune cells and immune subpopulations in the plantar skin at day 5 post UVB exposure in TRPA1 KO and wild type. **g-i.**

Flow cytometry quantification of the content of immune cells and immune subpopulations in the plantar skin at day 5 post UVB exposure in mice dosed daily with 40 mg/kg of Chembridge-5861528 or vehicle. Data plotted as Mean ± SEM with n=5 KO/6 WT mice/group (a-c.); n=8 mice/experimental group pooled from two independent experiments with same trend (d-f.); n=4 mice/experimental group (g-i.). KO: knock out.

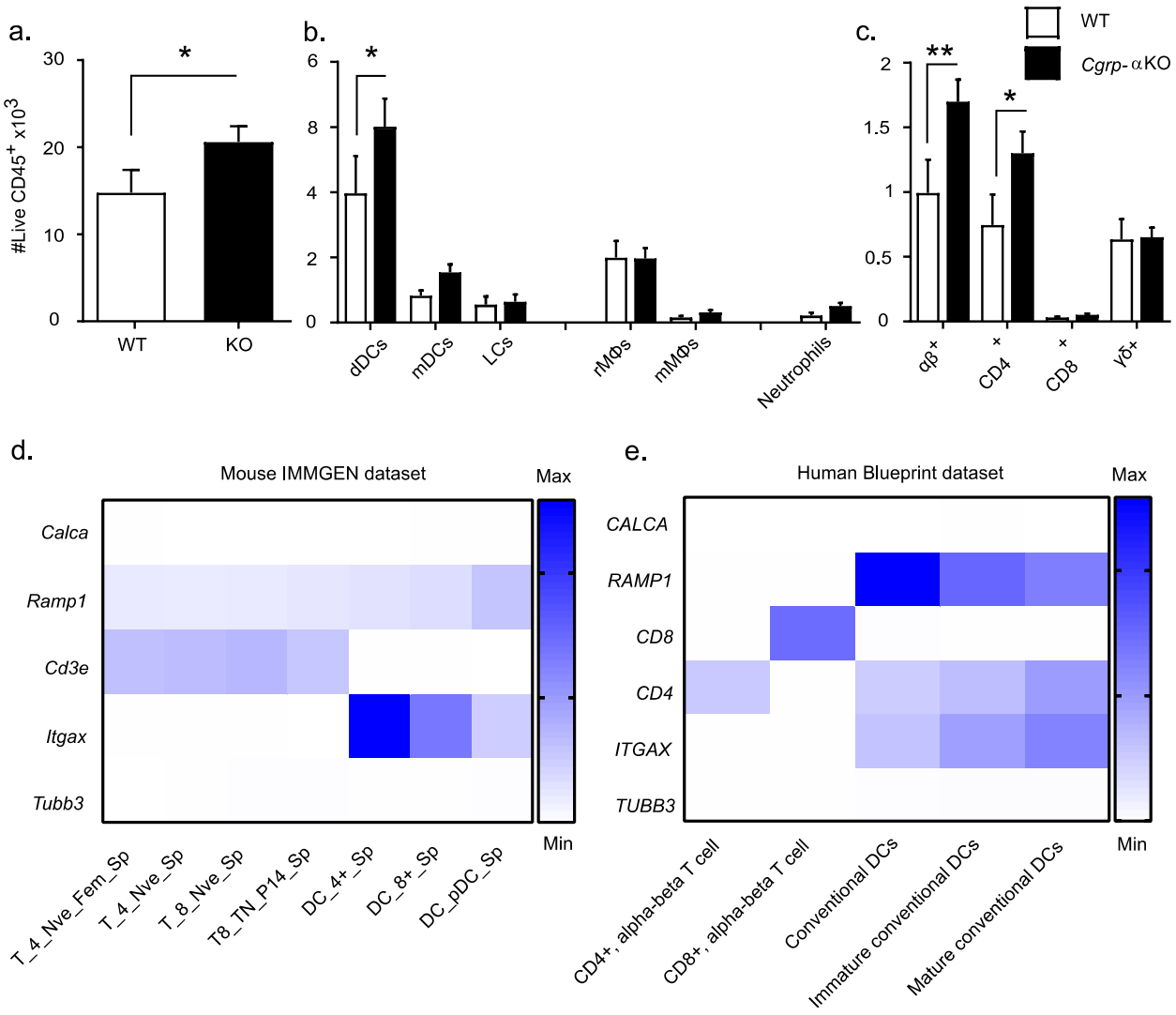

Figure 5. Ablation of the nociceptive neurotransmitter CGRP significantly affects the alterations caused by UVB irradiation at day 5 *in vivo*.

a-c. Flow cytometry quantification of the content of immune cell and immune cell subpopulations in the plantar skin at day 5 post UVB exposure in *Cgrp*-α KO and wild type mice. **d-e.** Analysis of publicly available transcriptome datasets for different subtypes of T cells and DCs to evaluate the expression of the neuropeptide CGRP (*Calca*), its receptor (*Ramp1*), immune cell markers (*Cd3d, Itgax, CD8, CD4*) and the neuronal specific control β3-tubulin (*Tubb3*). Heatmap rows show expression values normalized by DESeq2 (d.) or FPKM (e.). Columns define specific

immune cell types. Data plotted as Mean ± SEM with n=12 mice/group from three independent experiments pooled together. Multiple unpaired t-test followed by Holm-Sidak *post hoc* correction for multiple comparisons: *: p-value<0.05, **: p-value<0.01 (a-c.). KO: knock out.

SUPPLEMENTAL MATERIAL

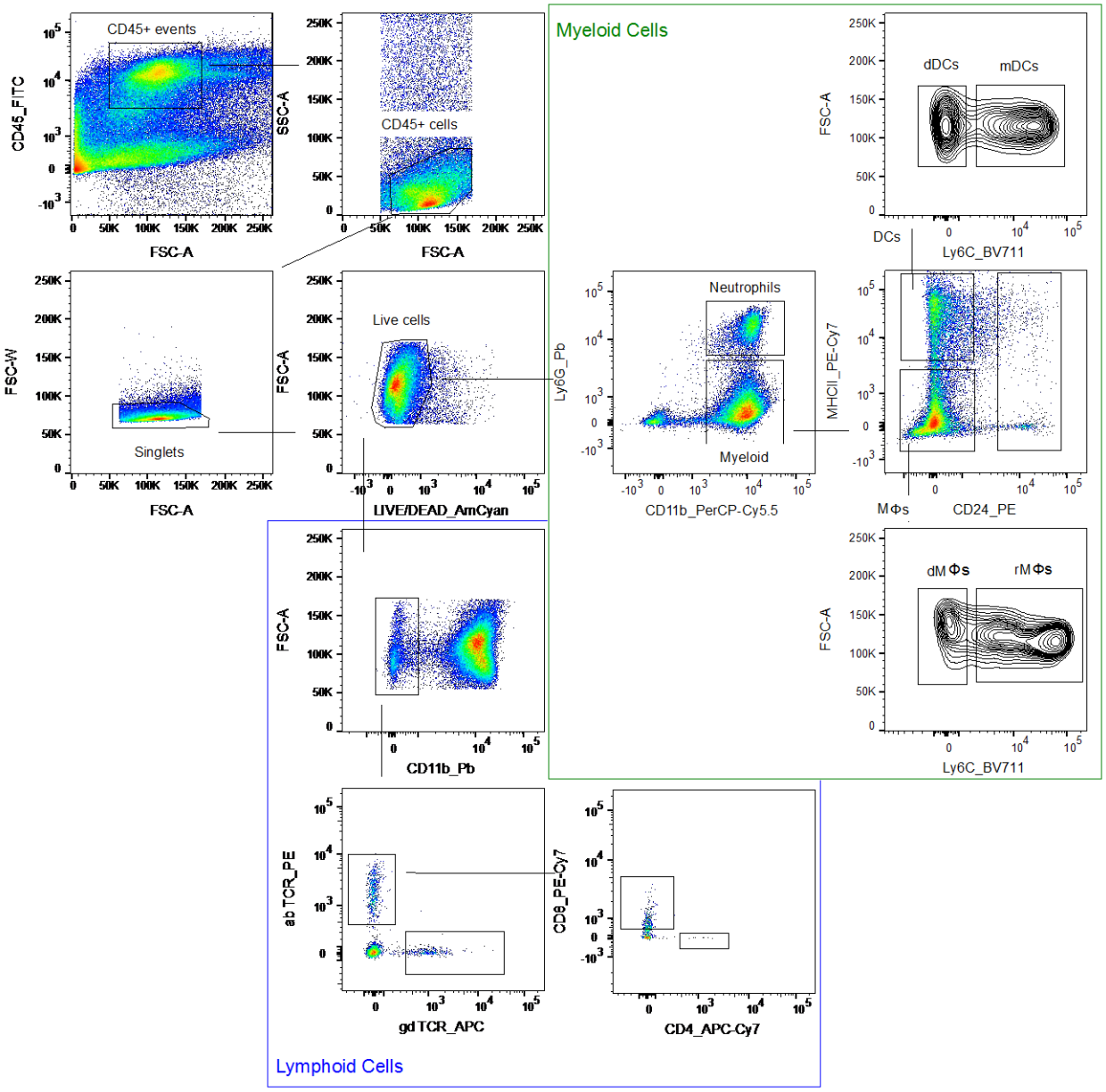

<u>Supplementary Figure 1. Flow cytometry gating strategy to discriminate cutaneous immune cell subpopulations in the murine plantar skin.</u> Representative flow cytometry dot plots defining the gating strategy used to discriminate immune cell subpopulations in the murine plantar skin. Immune cells were identified as $CD45^{+}$; single cells were discriminated plotting FSC area *vs* FSC width; live cells were gated as negative for live/dead staining; the different cell

subpopulations were identified based on combination of expression of surface markers and include neutrophils as $CD11b^{+}/Ly6G^{+}$; Langerhans cells (LCs) as $CD11b^{+}/ Ly6G^{-}/CD24^{+}/MHCII^{-\ to\ +}$; dermal DCs (dDCs) as $CD11b^{+}/Ly6G^{-}/CD24^{-}/MHCII^{+}/Ly6C^{-}$; monocyte-derived DCs (mDCs) as $CD11b^{+}/Ly6G^{-}/CD24^{-}/MHCII^{+}/Ly6C^{+}$; resident MΦs (rMΦs) as $CD11b^{+}/Ly6G^{-}/CD24^{-}/MHCII^{-}/Ly6C^{-}$ and monocyte-derived MΦs (mMΦs) as $CD11b^{+}/Ly6G^{-}/CD24^{-}/MHCII^{-}/Ly6C^{+}$; and lymphoid cells including $\alpha\beta^{+}$ T cells as $CD11b^{-}/\alpha\beta\ TCR^{+}$; $CD4^{+}$ T cell as $CD11b^{-}/\alpha\beta\ TCR^{+}/CD8^{-}/CD4^{+}$; $CD8^{+}$ T cells as $CD11b^{-}/\alpha\beta\ TCR^{+}/CD4^{-}/CD8^{+}$; and $\gamma\delta^{+}$ T cells as $CD11b^{-}/\alpha\beta\ TCR^{-}/\gamma\delta\ TCR^{+}$.

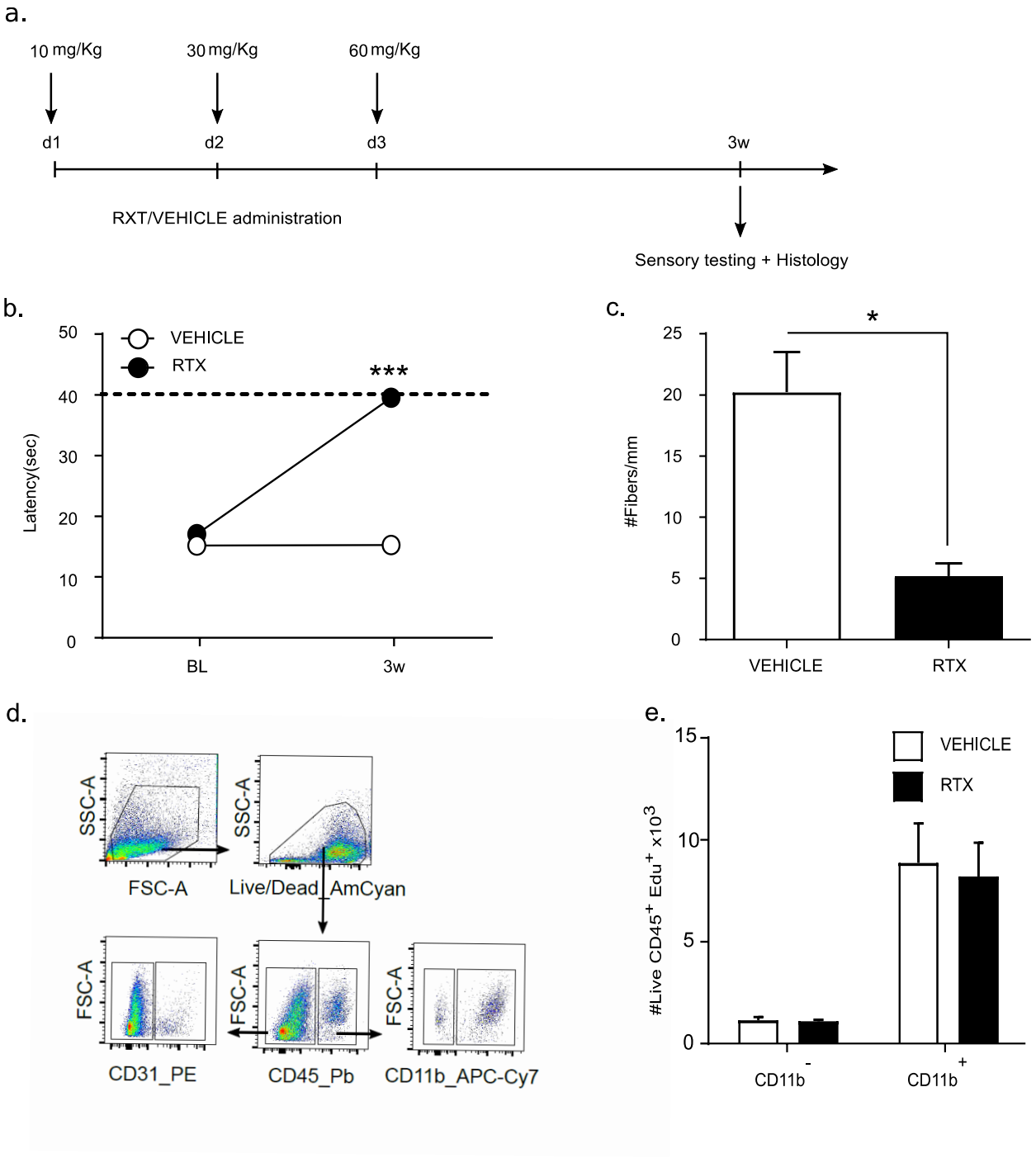

Supplementary Figure 2. RTX treatment causes cutaneous denervation *in vivo*. **a.** Schematic representing the experimental timeline. **b.** Hot plate testing to assess development of hyposensitivity to noxious thermal stimulation (dotted line=cut off). **c.** Quantification of plantar skin intraepidermal nerve fiber density by immunofluorescence. **d.** Sorting gating strategy to

discriminate cutaneous cell subpopulations from naïve plantar skin including myeloid cells ($CD45^+/CD11b^+$); lymphoid cells ($CD45^+/CD11b^-$); endothelial cells (ECs; $CD45^-/CD31^+$) and keratinocytes (KCs; $CD45^-/CD31^-$). **e.** Proliferation assay performed following administration of the intercalant EdU. Data plotted as Mean ± SEM with n=8 mice/experimental group (b.) and n=4 mice/group (c-d.); and n=5 mice/group (e.). Two-Way ANOVA with repeated measures followed by Bonferroni *post hoc* correction for multiple comparisons: ***: *p*-value < 0.001 (b.). Mann-Withney t-test: *: *p*-value < 0.05 (c.).

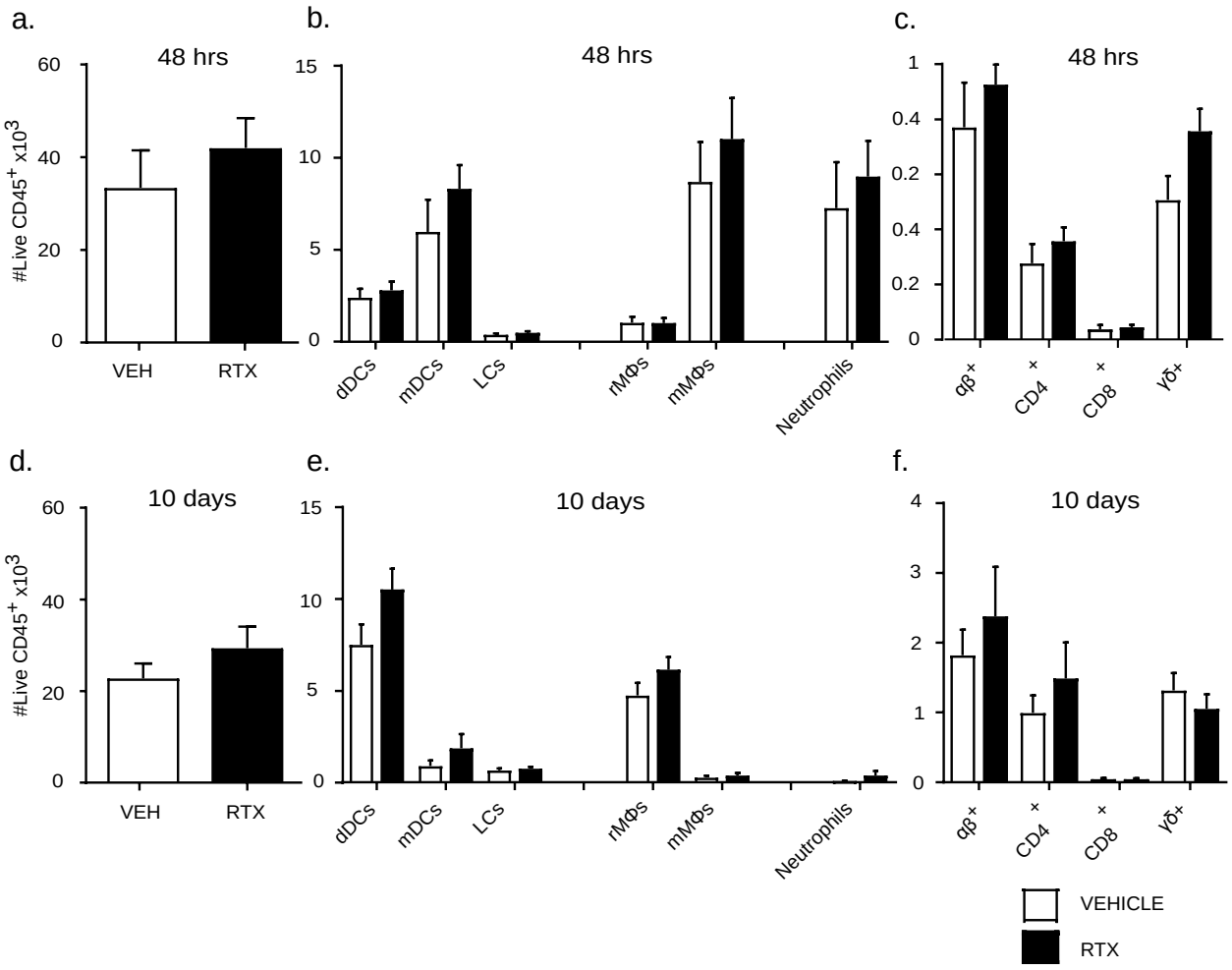

Supplementary Figure 3. RTX treatment does not affect cellular alterations caused by UVB irradiation at either 48 hrs or 10 d post exposure *in vivo*. **a-c.** Flow cytometry quantification of the content of immune cells at 48 hrs post UVB in RTX and vehicle treated mice. **d-f.** Flow cytometry quantification of the content of immune cells at 10 d post UVB in RTX and vehicle treated mice. Data shown as Mean ± SEM with n=5 mice/group/time point and representative of two independent experiments.

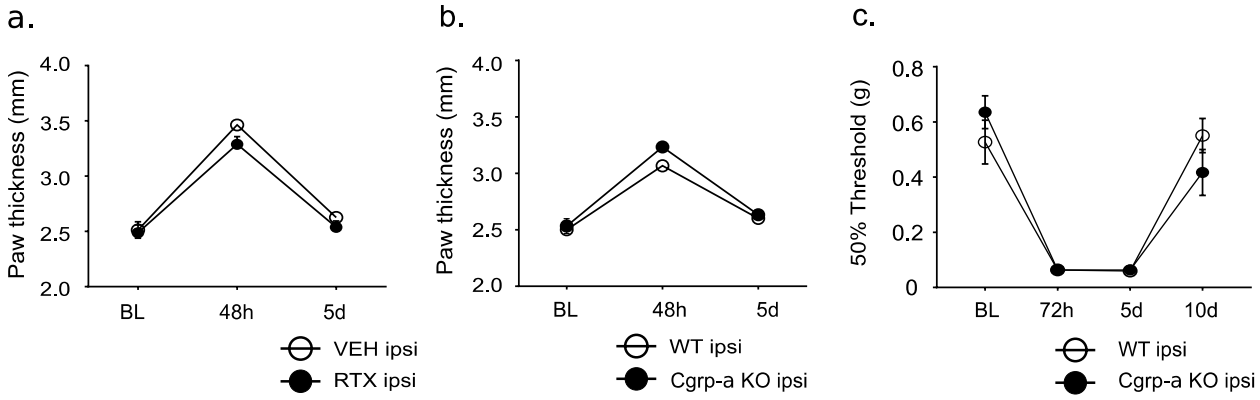

Supplementary Figure 4. Disruption of sensory neurons or CGRP expression do not affect edema or mechanical hyperalgesia *in vivo*. a-b. Time course of changes in edema measured as paw thickness in RTX and vehicle-treated mice (**a.**) as well as Cgrp-α KO and WT mice (**b.**). **c.** Time course of changes in sensitivity to mechanical stimulation measured as the amount of pressure required to induce withdrawal of the tested paw in 50% of the assessment. Data plotted as Mean ± SEM with n=8 mice/time point.